

Switching magnetization of quantum antiferromagnets: Schwinger boson mean-field theory compared to exact diagonalization

Florian Johannesmann,^{1,*} Asliddin Khudoyberdiev,^{1,†} and Götz S. Uhrig^{1,‡}

¹*Condensed Matter Theory, TU Dortmund University,
Otto-Hahn-Straße 4, 44227 Dortmund, Germany*

(Dated: January 9, 2026)

Antiferromagnets have attracted significant attention because of their considerable potential in engineering high-density and ultrafast memory devices, a crucial and increasingly demanded component of contemporary high-performance information technology. Theoretical and experimental investigations are actively progressing to provide the capability of efficient switching and precise control of the Néel vector, which is crucial for the intended practical applications of antiferromagnets. Recently, a time-dependent Schwinger boson mean-field theory has been successfully developed to study the sublattice magnetization switching in anisotropic quantum antiferromagnets [K. Bölsmann *et al.*, [PRX Quantum 4, 030332 \(2023\)](#)]. Here we use a complementary exact diagonalization method to study such sublattice magnetization switching, but in small-cluster quantum antiferromagnets, by means of an external magnetic field. Furthermore, this article aims to support the findings of the Schwinger boson approach. We show that the results of both approaches are consistent at short time scales, with only about 12.5 % deviations. The consistency of the outcomes obtained through this alternative exact approach demonstrates that the time-dependent Schwinger boson mean-field theory is a versatile framework to capture the essentials of the switching process in quantum antiferromagnets. Thereby, the findings of current article pave the way for further theoretical and computational progress in the study of antiferromagnets for engineering spintronic devices with ultrahigh density and ultrafast speed.

I. INTRODUCTION

The manipulation and control of magnetization in magnetic materials is of great interest in many areas of physics due to their applications for high-density memories and spintronic devices [1, 2]. Moreover, experimental evidence suggests that antiferromagnetic materials combined with heavy metal layers can be used as spintronic terahertz (THz) emitters [3, 4]. Therefore, antiferromagnets have been proposed as a promising platform because of their ultrafast spin dynamics compatible with ultrafast information processing, robustness against external noise fields and absence of stray fields between the domains [5–7]. Research is currently underway to determine the viability of employing antiferromagnets for information storage and processing [8, 9].

In antiferromagnets, the absence of net magnetization poses a substantial obstacle to the effective readout and manipulation of the direction of the Néel vector. However, intense theoretical [10–15] and experimental [16–19] research is currently underway, with significant progress in recent years to demonstrate the possibility of efficient switching [19–22], read-out [9, 23, 24] and full control [25–27] of the antiferromagnetic order, to make it practically applicable.

The experimental observation of deterministic electrical 180° switching of the Néel vector in the spin-split antiferromagnet Mn_5Si_3 was achieved through utilization

of a spin-orbit torque with an asymmetric energy barrier [21]. In this experiment, the read-out of the Néel vector switching is realized through the flipping the sign of the anomalous Hall conductivity. This even made the fabrication of an antiferromagnetic device possible with both high ("0" state) and low ("1" state) resistance, thereby enabling the realization of robust write and read-out cycles [21]. Moreover, atomistic spin simulations confirm the considered switching processes [21]. Similarly, current-induced spin-orbit torques enabled full switching of the Néel vector in antiferromagnet $(\text{Fe},\text{Co})_3\text{GaTe}_2$ with perpendicular magnetic anisotropy [22]. Very recently, Jourdan *et al.* [28] even highlighted experimentally two distinct mechanisms using a current pulse for switching the sublattice magnetization in the antiferromagnet Mn_2Au . The authors concluded that current-induced heating (thermomagnetoelastic effect) drives the Néel vector switching under 10 μs pulses, while the Néel spin-orbit-torque [18, 19, 29] is responsible for complete reorientation under pulses shorter than 100 ns, as required for ultrafast applications. Consequently, one can conclude that the state-of-the-art antiferromagnetic switching has undergone significant progress in the experimental domain.

Clearly, this calls for further theoretical support. So far, the switching mechanism was primarily studied for classical vectors by the Landau-Lifshitz-Gilbert equation [11, 30] which can be linked to the quantum Lindblad formalism [31] or similarly by atomistic spin dynamics simulations [21, 32] which include thermal fluctuations on a stochastic level. Our objective is to raise the theoretical description to the quantum level. In equilibrium, spin wave theory at face value or in a self-consistent way

* florian.johannesmann@tu-dortmund.de

† asliddin.khudoyberdiev@tu-dortmund.de

‡ goetz.uhrig@tu-dortmund.de

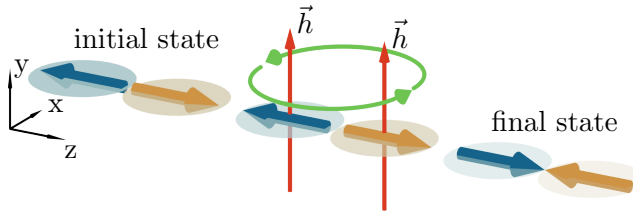


FIG. 1. Illustration of the manipulation of the sublattice magnetization. The initial state is shown on the left with two linked sublattices. The arrows in the circles show the sublattice magnetization direction. A uniform magnetic field is applied to switch the order (shown in the middle) and the final switched state is obtained (shown on the right). Round green arrows indicate the Larmor precession of the sublattice spins.

allow one to incorporate the leading quantum corrections. The standard choices of the Holstein-Primakoff representations [33] or Dyson-Maleev representation [34, 35] only capture the fluctuations around a static, prechosen order. Thus, they cannot capture strong deviations such as they occur in the re-orientation of the magnetization, except in very tedious considerations [36]. Thus, we choose the Schwinger boson representation [37].

The time-dependent Schwinger boson mean-field theory (SBMFT) has been developed to study switching in quantum antiferromagnets driven by external magnetic fields [12–14, 38]. This approach successfully demonstrated that control of the Néel vector can be achieved by applying strong uniform fields (Fig. 1) [12, 13]. It was shown that the size of the spin gap in the dispersion determines the strength of the uniform external field required for the switching. Time-dependent control fields allow for the reduction of the strength of the required switching field due to resonant control [13]. Moreover, staggered magnetic fields on neighboring sublattices generate exchange field enhancement, so that switching occurs for significantly lower fields [14], similar to the effect of Néel spin-orbit torque.

Even though the quantum system is treated to be a closed system, the dynamics of sublattice magnetization after switching is not fully coherent, but a slow decay of the oscillations is observed. This phenomenon is due to dephasing caused by the numerous modes at different frequency in the system [12–14, 38]. Furthermore, considering an open quantum system by including spin-lattice relaxation, derived from the Lindblad formalism [39], an exponential decay of the oscillations and fast convergence to the steady-state after full ultrafast switching have been observed [38]. Therefore, the methodological progress to deal with Schwinger mean-fields including Lindblad dissipators facilitated also to address the differences between dephasing and spin-lattice relaxation in true switching processes. But still, to validate the results derived so far either classically or by quantum mean-field approaches,

the use of additional quantum approaches is necessary.

In this work, we report results obtained from the complementary exact diagonalization (ED) method in small clusters to simulate switching processes in antiferromagnets by means of external magnetic fields. We consider different two-dimensional antiferromagnetic clusters with spin-1/2 sites, as approximations for the infinite two-dimensional square lattice, see below.

We emphasize that the comparison of mean-field results to small cluster ED results is an intricate task: The mean-field approach easily allows to describe rather large systems and there is little difficulty to capture symmetry breaking. The ED approach, however, is limited to rather small systems of $\mathcal{O}(20)$ spins which do not show any symmetry breaking due to quantum tunneling, see for instance Ref. [40]. To generate sublattice magnetization which makes it possible to address the switching process at all, some initial state preparation with small staggered fields cannot be circumvented.

The paper is organized in the following manner. In section II, we provide a brief description of time-dependent SBMFT and a detailed discussion of the exact diagonalization method. Section III reports the results of the exact diagonalization method and its comparisons with the findings of SBMFT. The conclusions and perspectives of our work are reported in section IV. The details about the initialization of systems and the structure of clusters are provided in the Appendix.

II. MODEL AND METHOD

We start with a system described by the Heisenberg model on a square lattice with Hamiltonian

$$\mathcal{H}_0 = J \sum_{\langle i,j \rangle} \left[\frac{\chi}{2} (S_i^+ S_j^- + S_i^- S_j^+) + S_i^z S_j^z \right] - h_z \sum_i (-1)^i S_i^z \quad (1)$$

where χ is an anisotropy parameter, J the exchange coupling, and $h_z = g\mu_B B_z$ an external field in energy units. Here, g is the Landé g -factor, μ_B is the Bohr magneton, and B_z is the external magnetic field along the z axis. Subsequent analyses of the results employ energies measured in units of the antiferromagnetic exchange coupling $J > 0$. We want to perform exact diagonalization calculations on small clusters to corroborate the SBMFT results on switching [12] by capturing the main quantum effects at zero temperature. Therefore, we included a Zeeman term with an staggered tiny auxiliary field in the z direction in Eq. (1) to force antiferromagnetically alignment of the spins [41]. Otherwise, the total spin of the ground state is zero and no spin direction is singled out [42]. Thus, the auxiliary field is necessary for small cluster sizes to obtain a ground state with proper finite values of sublattice magnetization [43] by counteracting quantum tunneling between the two states of long-range order in easy-axis spin systems, see Fig. 2 and for instance Ref. [40]. Even for a robust convergence

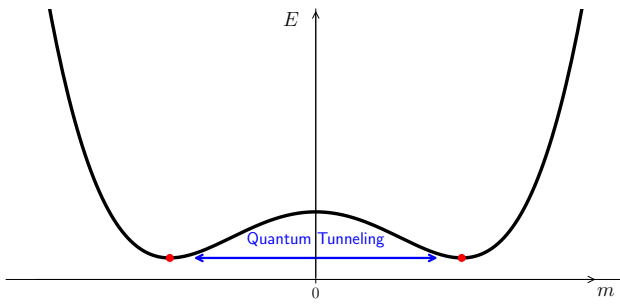


FIG. 2. Illustration of quantum tunneling between two ordered states, depicted as red dots, separated by an intermediate activation energy, drawn as a solid black line.

of self-consistency equations of the mean-field the auxiliary field is indicated [44] to determine the orientation of the symmetry breaking [12]. For diverging system size, the necessary auxiliary fields vanish.

Below, we will briefly recap SBMFT, then provide details of our ED approach.

A. Schwinger boson mean-field approximation

The switching of the antiferromagnetic order implies more than small fluctuations around the ordered state. In order to analyze the switching processes in antiferromagnets, the SU(2) Schwinger boson representation is the most suitable [12–14, 38] due to its capability to describe spin-symmetric phases as well [44]. In the SU(2) Schwinger boson representation, the spin operators of the Heisenberg Hamiltonian are replaced by two flavors of bosonic operators as

$$\mathbf{S}_i = \frac{1}{2} (a_i^\dagger b_i^\dagger) \boldsymbol{\sigma} \begin{pmatrix} a_i \\ b_i \end{pmatrix}, \quad (2)$$

where $\boldsymbol{\sigma}$ is the Pauli vector. To perform a meaningful mapping of the physical spin Hilbert space to the subspace of the bosonic Hilbert space, one limits the Schwinger boson occupation at each site to be

$$a_i^\dagger a_i + b_i^\dagger b_i = 2S, \quad (3)$$

where S is the spin length. Then, two Schwinger bosons span the physical Hilbert space for $S = 1/2$ as $|1, 0\rangle := |\uparrow\rangle$ and $|0, 1\rangle := |\downarrow\rangle$. Other linear combinations of the bosons can represent other spin orientations in the sublattice. The sublattice magnetization is calculated by

$$m_z = \langle S_i^z \rangle = \frac{1}{2} (\langle a_i^\dagger a_i \rangle - \langle b_i^\dagger b_i \rangle). \quad (4)$$

Prior to the substitution of the spin operators with bosonic operators in Eq. (1), it is advantageous to introduce the bond operators as $A_{ij} := a_i b_j - b_i a_j$ and

$B_{ij} := a_i b_j + b_i a_j$, which enable rewriting the Hamiltonian in a compact form as

$$\mathcal{H}_0 = -\frac{1}{4} \sum_{\langle i,j \rangle} \left\{ (1 + \chi) A_{ij}^\dagger A_{ij} + (1 - \chi) B_{ij}^\dagger B_{ij} - 4S^2 \right\} - \frac{h_z}{2} \sum_i (-1)^i (a_i^\dagger a_i - b_i^\dagger b_i). \quad (5)$$

The bond operator A_{ij} is an antisymmetric to the interchange of $i \rightarrow j$. To simplify analytical calculations, we perform a 180° spin rotation on one sublattice about the y axis which amounts to a unitary transformation not affecting physics. As a result, the bond operators become symmetric as $A_{ij} := a_i a_j + b_i b_j$ and $B_{ij} := a_i a_j - b_i b_j$, and we retain the full translational invariance of the Hamiltonian. The alternating field h_z also becomes a uniform field, which simplifies the calculations significantly. Additionally, the mean-field approximation - the primary tool employed in the subsequent subsection, becomes compactly applicable even in the SU(2) representation, e.g., $A_{ij}^\dagger A_{ij} \approx A_{ij}^\dagger \langle A_{ij} \rangle + A_{ij} \langle A_{ij}^\dagger \rangle - \langle A_{ij}^\dagger \rangle \langle A_{ij} \rangle$ [44–46]. This scheme is justified by an expansion in the inverse number of flavors, here two. It is not identical to Wick’s theorem, though bearing similarities.

The mean-field Hamiltonian in momentum space reads

$$\mathcal{H}_0^{\text{MF}} = E_0 - \frac{1}{2} \sum_{\mathbf{k}} \gamma_{\mathbf{k}} (C_- a_{\mathbf{k}}^\dagger a_{-\mathbf{k}}^\dagger + C_+ b_{\mathbf{k}}^\dagger b_{-\mathbf{k}}^\dagger + C_-^* a_{\mathbf{k}} a_{-\mathbf{k}} + C_+^* b_{\mathbf{k}} b_{-\mathbf{k}}) + \left(\lambda - \frac{h_z}{2} \right) \sum_{\mathbf{k}} a_{\mathbf{k}}^\dagger a_{\mathbf{k}} + \left(\lambda + \frac{h_z}{2} \right) \sum_{\mathbf{k}} b_{\mathbf{k}}^\dagger b_{\mathbf{k}}, \quad (6)$$

where $C_{\pm} := A(1 + \chi) \mp B(1 - \chi)$ and $C_{\pm}^* := A^*(1 + \chi) \mp B^*(1 - \chi)$ with $A := \langle a_i a_j + b_i b_j \rangle$, $B := \langle a_i a_j - b_i b_j \rangle$ and $A^* := \langle a_i^\dagger a_j^\dagger + b_i^\dagger b_j^\dagger \rangle$, $B^* := \langle a_i^\dagger a_j^\dagger - b_i^\dagger b_j^\dagger \rangle$. In our notation the parameters C_- and C_+ correspond to the bosons a and b , respectively. The constant E_0 is a constant energy and $\gamma_{\mathbf{k}} = \frac{1}{4} \sum_{\delta} e^{i\mathbf{k} \cdot \delta}$. The Lagrange term with the Lagrange parameter λ is included in the Hamiltonian to fix the average number of bosons per lattice site according to the constraint in Eq. (3).

Next, we diagonalize the mean-field Hamiltonian using Bogoliubov transformations and obtain the dispersion relations for the bosonic flavors

$$\omega_{\mathbf{k}}^{\pm} = \sqrt{\left(\lambda \pm \frac{h_z}{2} \right)^2 - (|C_{\pm}| \gamma_{\mathbf{k}})^2}. \quad (7)$$

Because of simulations of finite size clusters, both bosons acquire an energy gap as

$$\Delta^{\pm} = \omega_{\mathbf{k}=0}^{\pm}. \quad (8)$$

The closed set of self-consistent mean-field equations is constructed using the mean-field parameters and the con-

straint in Eq. (3) as

$$A = \langle a_i a_j \rangle + \langle b_i b_j \rangle = \frac{1}{N} \sum_{\mathbf{k}} \gamma_{\mathbf{k}} (\langle a_{\mathbf{k}} a_{-\mathbf{k}} \rangle + \langle b_{\mathbf{k}} b_{-\mathbf{k}} \rangle), \quad (9a)$$

$$B = \langle a_i a_j \rangle - \langle b_i b_j \rangle = \frac{1}{N} \sum_{\mathbf{k}} \gamma_{\mathbf{k}} (\langle a_{\mathbf{k}} a_{-\mathbf{k}} \rangle - \langle b_{\mathbf{k}} b_{-\mathbf{k}} \rangle), \quad (9b)$$

$$2S = \langle a_i^\dagger a_i \rangle + \langle b_i^\dagger b_i \rangle = \frac{1}{N} \sum_{\mathbf{k}} (\langle a_{\mathbf{k}}^\dagger a_{\mathbf{k}} \rangle + \langle b_{\mathbf{k}}^\dagger b_{\mathbf{k}} \rangle), \quad (9c)$$

where

$$\langle a_{\mathbf{k}}^\dagger a_{\mathbf{k}} \rangle = \frac{1}{2} \left(\frac{\lambda - \frac{h_z}{2}}{\omega_{\mathbf{k}}^-} - 1 \right), \quad (10a)$$

$$\langle b_{\mathbf{k}}^\dagger b_{\mathbf{k}} \rangle = \frac{1}{2} \left(\frac{\lambda + \frac{h_z}{2}}{\omega_{\mathbf{k}}^+} - 1 \right), \quad (10b)$$

$$\langle a_{\mathbf{k}} a_{-\mathbf{k}} \rangle = \frac{C - \gamma_{\mathbf{k}}}{2\omega_{\mathbf{k}}^-}, \quad (10c)$$

$$\langle b_{\mathbf{k}} b_{-\mathbf{k}} \rangle = \frac{C + \gamma_{\mathbf{k}}}{2\omega_{\mathbf{k}}^+}. \quad (10d)$$

We prepare the initial state such that there are more a bosons than b bosons [12], i.e., the initial sublattice magnetization is finite and positive. The self-consistent equations (9) are solved to find the mean-field parameters and the Lagrange parameter, which completes the initialization.

The system is driven through the magnetic field along the y axis to reach the reorientation of the Néel vector

$$\mathcal{H}_m = -h_y \sum_i S_i^y = -\frac{h_y}{2i} \sum_{\mathbf{k}} (a_{\mathbf{k}}^\dagger b_{\mathbf{k}} + b_{\mathbf{k}}^\dagger a_{\mathbf{k}}), \quad (11)$$

where $h_y = g\mu_B B_y$. The above Hamiltonian does not commute with the mean-field Hamiltonian in Eq. (6). Therefore, the time evolution of the expectation values of bilinear operators are computed using the Heisenberg equation of motion, and a closed set of differential equations are constructed using the full mean-field Hamiltonian $\mathcal{H}_t = \mathcal{H}_0^{\text{MF}} + \mathcal{H}_m$ [12–14]. Note that also the Lagrange parameter λ needs to be made time-dependent to keep the constraint fulfilled in the course of the evolution [14, 47]. Lastly, the differential equations are solved at each momentum point \mathbf{k} in the Brillouin zone, where the solutions enable the analyzes of the dynamics of the magnetization as

$$m_z(t) = \frac{1}{2} (\langle a_i^\dagger a_i \rangle - \langle b_i^\dagger b_i \rangle) = \frac{1}{2N} \sum_{\mathbf{k}} (\langle a_{\mathbf{k}}^\dagger a_{\mathbf{k}} \rangle - \langle b_{\mathbf{k}}^\dagger b_{\mathbf{k}} \rangle), \quad (12)$$

with N denoting the number of lattice sites.

B. Exact diagonalization

For the exact diagonalization (ED) we start from the Hamiltonian in Eq. (1). In order to take full advantage of the translational symmetry of the underlying lattice, one sublattice, designated as j , is rotated about the spin S_y axis as for the mean-field treatment. The rotated Hamiltonian now reads

$$\mathcal{H}_R = -J \sum_{<i,j>} \left[\frac{\chi}{2} (S_i^+ S_j^+ + S_i^- S_j^-) + S_i^z S_j^z \right] - h_z \sum_i S_i^z. \quad (13)$$

Regarding the system size, we use translational symmetries in order to reduce the effective Hilbert space dimension to reach a maximum number of 24 spins. For the simulations, we use the software package QuSpin [48, 49] that supports symmetry operations and efficient run time and memory performance. The ground state search is done by using a sparse eigen-solver that runs an implicitly restarted Lanczos algorithm within the subspace $H_{(k_x, k_y)}$ with momentum quantum numbers $(k_x = 0, k_y = 0)$. For the time evolution of the magnetization, we solve the time-dependent Schrödinger equation by using a high order Runge Kutta method. We compare the short-time magnetization dynamics and the required switching fields at different easy-axis anisotropy strengths to the results of the SBMFT. The correspondence of the results of two different approaches allows for a cautious confirmation of the results of time-dependent SBMFT [12–14].

The first step is to determine a suitable ground state in the method that can serve as an initial state with finite sublattice magnetization for the time evolution. Therefore, a suitable h_z field is necessary and must be found in the first place. According to Marshall's theorem [44], the ground state of the Hamiltonian is located in the symmetry reduced subspace $H_{(k_x, k_y)}$ with momentum quantum numbers $(k_x = 0, k_y = 0)$. For several h_z values, the ground state and the corresponding magnetization of one spin of the lattice is calculated. The obtained values are then fitted with a hyperbolic ansatz for the magnetization curve

$$m_z(h_z) = a \cdot \tanh \left(\frac{b \cdot h_z}{1 + c \cdot h_z} \right), \quad (14)$$

where a, b and c are fit parameters. The parameter a can be thought of as the magnetization reached at an infinitely large field. A suitable value for h_z is obtained by setting the normalized derivative of the fit function to 0.03 as

$$m_z'(h_z) = \frac{1}{\cosh^2 \left(\frac{b \cdot h_z}{1 + c \cdot h_z} \right) (1 + c \cdot h_z)^2} \stackrel{!}{=} 0.03. \quad (15)$$

An example of the fit procedure is shown in Fig. 3 for a 4×4 cluster. In this way, we determine a suitable value of the auxiliary staggered field h_z , further details are given in App. A.

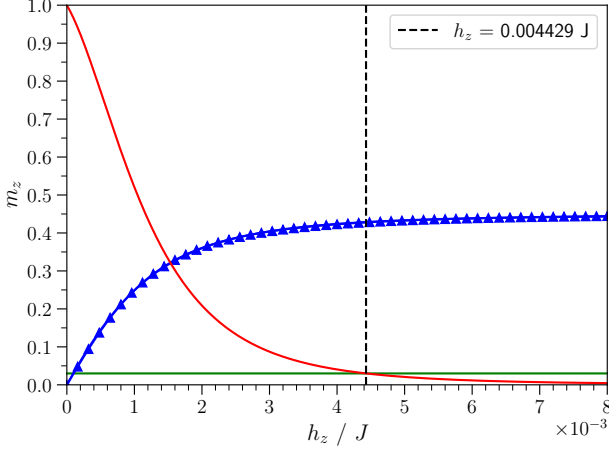


FIG. 3. Sublattice magnetization values (blue dots) dependent on the h_z field for a 4×4 cluster at $\chi = 0.6$, fitted with the hyperbolic ansatz (14) (solid blue curve). The normalized derivative is shown as a red solid line and the threshold value of 0.03 is depicted as a green horizontal line. The estimated initial h_z field is shown as a vertical dotted black line.

For the time evolution of the magnetization, the ground state is initialized with the calculated auxiliary h_z field. For $t > 0$, h_z is turned off and the switching field h_y is applied to the system. Then, the Hamiltonian reads

$$\mathcal{H}_t = -J \sum_{\langle i,j \rangle} \left[\frac{\chi}{2} (S_i^+ S_j^+ + S_i^- S_j^-) + S_i^z S_j^z \right] - h_y \sum_i S_i^y. \quad (16)$$

Note that the field in y direction is uniform before and after the sublattice rotation because the rotation was done around the y direction so that this spin component is not changed.

Since the ground state lies within the subspace $H_{(0,0)}$ and the Hamiltonian \mathcal{H}_t is also translationally invariant, the time evolution itself is restricted to this subspace. The time evolution is calculated using QuSpin [48, 49] by solving the time dependent Schrödinger equation using a Runge Kutta method, called dop853, of order 8.

Since the h_z field is turned off for $t > 0$ the initial state is no longer an eigenstate, but will display some time dependence which we consider spurious. It cannot be avoided unfortunately since we need initial states with finite sublattice magnetization. This spurious time dependence is rather slow, at least for small enough values of χ where the quantum tunneling is weak, see Fig. 4. This effect is not very detrimental because the actual switching will be significantly faster. We will focus on intermediate values of anisotropy $\chi \in (0.3, 0.8)$ where the quantum tunneling, sketched in Fig. 2, is indeed weak for the accessible cluster sizes.

To quantify the degree of quantum tunneling we show the energy gap between the two lowest eigenstates with the same total spin $S = 0$ in the upper panel of Fig. 5.

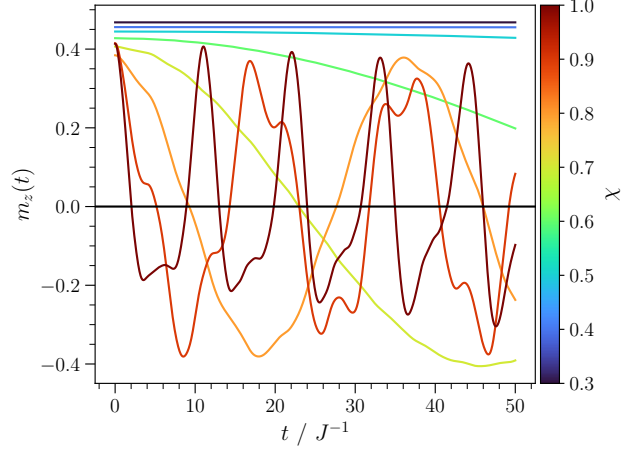


FIG. 4. Spurious dynamics of the magnetization for a 4×4 cluster after the auxiliary h_z field has been turned off at $t > 0$. We point out that this spurious evolution becomes progressively slower with increasing system size because the required auxiliary fields become smaller.

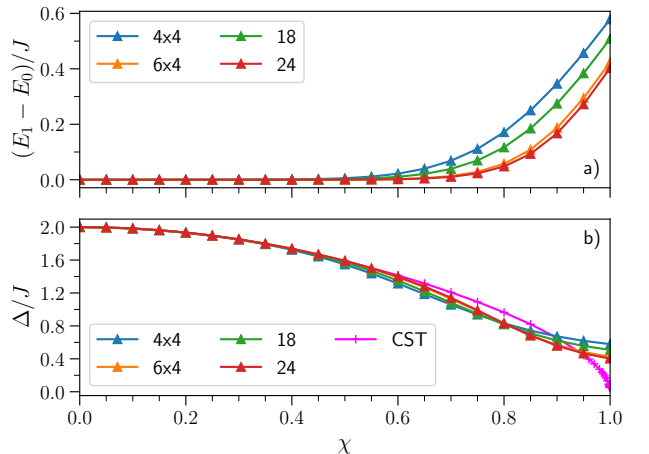


FIG. 5. Results of ED calculations: panel a) Energy difference between the ground state E_0 and the first excited E_1 state in the subspace of total spin $S = 0$. Panel b) Minimal energy required for one spin flip, i.e., for $\Delta S = 1$, compared to CST data [43]. In both cases, no external h_z field is applied. The clusters are given explicitly in App. B.

The matrix element of quantum tunneling is proportional to the energy splitting of the two lowest eigenvalues. It becomes negligible for small values of χ and decreases for larger clusters. Panel b) displays the conventional spin gap for comparison which is accompanied by a change of spin from $S = 0$ to $S = 1$.

Through the additional h_y field the magnetization is switched from $m_z > 0$ to $m_z < 0$. Our condition for the threshold of the switching field is set to be the h_y value at which the first minimum of the magnetization curve touches $m_z = 0$. This is done by using a Brent bisection

method. In each iteration of h_y the time evolution of the magnetization is calculated for discrete time points, then interpolated by a cubic spline and the first minimum of that function is computed.

III. RESULTS

We simulate various cluster of rectangular and of rhombic shape, see App. B. During the initialization phase, we use the same h_z fields for both ED and SBMFT which depends on the anisotropy parameter χ to compare and to conduct the analyses of the system's dynamics induced by a switching field h_y .

The ground state of a finite quantum antiferromagnet without any external field applied, as determined by ED, is a superposition of all the states in the subspace of total magnetization $M = 0$. This can be viewed as the effect of quantum tunneling. Thus, ED is unable to demonstrate switching in a direct manner because of the lack of spontaneous magnetization. We incorporate an explicit symmetry-breaking term, which is achieved by introducing a Zeeman term, with a reasonably chosen small auxiliary h_z field. Consequently, the cluster is initialized with non-degenerate low-energy states displaying finite sublattice magnetization.

A. The dynamics of the magnetization

To set the stage, we present the results of SBMFT for a relatively large system of 500×500 sites. Figure 6(a) shows the dynamics of the occupation numbers of a and b bosons together with the resulting sublattice magnetization according to Eq. (12). As mentioned in the Sect. II A, there are initially more a bosons than b bosons in the sublattice. To ensure proper convergence of self-consistency equations, we apply a small auxiliary field $h_z = 1.329 J N^{-1}$ [12] initially. Then, the external driving field $h_y = 1.7 J$ manipulates the bosonic occupation number in the sublattice such that more b bosons replace a bosons while keeping the total number constant. The transition of magnetization takes place at the time point (vertical double-headed arrow in Fig. 6(a)) when these two bosonic flavors attain equal occupation. At later times, the magnetization becomes negative, i.e., the order switches from the \uparrow state to the \downarrow state, but with slowly decreasing oscillations after the switching. We attribute these evanescent oscillations to dephasing effects [38]. This is one of the key findings of the time-dependent SBMFT, particularly in the context of studying switching, as SBMFT is capable of capturing the quantum effect of dephasing. This effect does not occur in classical macrospin calculations.

Another important result is that magnetization never recovers its initial value in absolute terms. Its absolute value (the dashed green line in Fig. 6(a)) is not reached after reorientation because the control field increases the

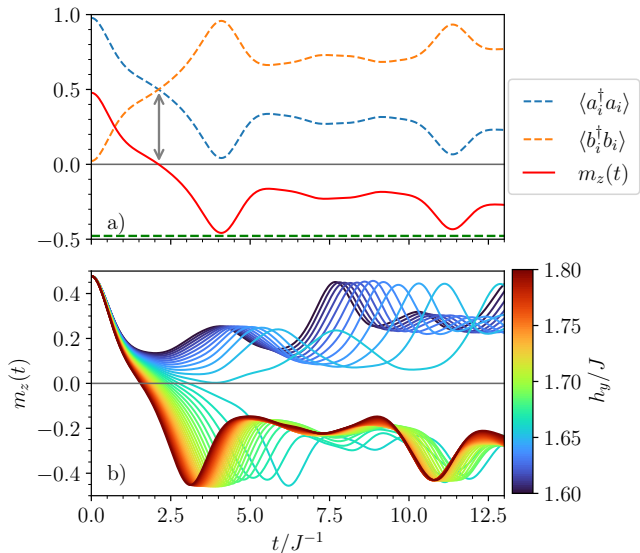


FIG. 6. Panel (a) shows the dynamics of the occupation of the Schwinger bosons $\langle a_i^\dagger a_i \rangle$ and $\langle b_i^\dagger b_i \rangle$ together with the resulting magnetization m from Eq. (12) for $h_y = 1.7 J$. The dashed green line shows the negative value of the initial magnetization $m_{z0} = m_z(t = 0)$. Panel (b) represents the dynamics of the magnetization for external switching fields in the interval $h_y \in [1.6 J, 1.8 J]$. Both graphs are the results of time-dependent SBMFT at $\chi = 0.5$.

total energy of the system so that the magnetization is pushed away from its initial values belong to its almost degenerate ground states. Note that the current model does not comprise any relaxation mechanisms [38].

Figure 6(b) illustrates the dynamics of the sublattice magnetization in response to an external magnetic field from the interval of $h_y \in [1.6 J, 1.8 J]$ at $\chi = 0.5$. It is easy to see that for small h_y fields no switching is obtained, whereas high switching fields result in a sign change in the sublattice magnetization. It has been established that a threshold value of the field, denoted as h_y^{thr} , is required to induce the desired transition [12–14, 50]. We emphasize that it is an interesting property of this switching process that the sublattice magnetization stays switched even though the switching fields $h_y > h_y^{\text{thr}} = 1.656 J$ is kept at all times $t > 0$. One could have expected that the sublattice magnetization starts to oscillate and keeps switching back and forth as would be the case for two macrospins [13, 30, 51]. The reason why this does not occur is dephasing which is important in large quantum systems because of the destructive interference of a macroscopic number of modes at all wave vectors \mathbf{k} . Dephasing is less pronounced in small quantum systems since there is not a large number of modes which can be superposed to reach destructive interference. Hence, one can expect that smaller quantum systems display more oscillations which do not fade away completely. This is particularly likely in the mean-field approach in which there is only one mode per momentum

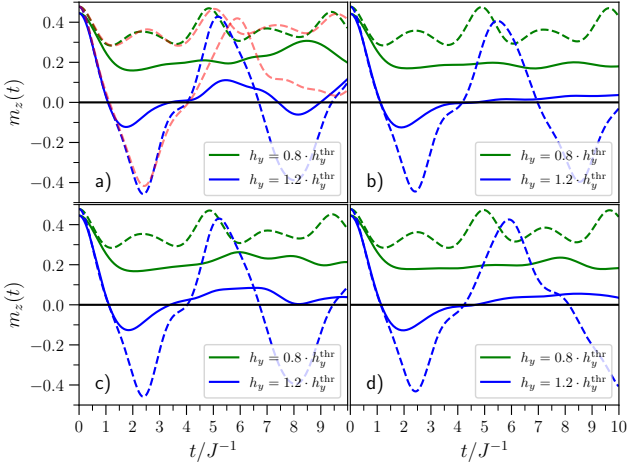


FIG. 7. Comparison of the magnetization dynamics of the results of ED (solid) and SBMFT (dashed) methods at $\chi = 0.5$. a) 4×4 , b) 6×4 , c) 18, d) 24. The h_y fields were chosen with respect to the threshold fields h_y^{thr} of the respective method. The red curve corresponds to the result of a 500×500 SBMFT cluster for comparison.

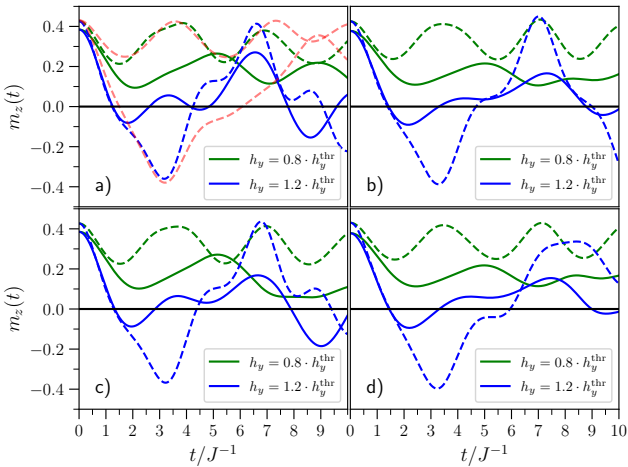


FIG. 8. Comparison of the magnetization dynamics of the results of ED (solid) and SBMFT (dashed) methods at $\chi = 0.8$. a) 4×4 , b) 6×4 , c) 18, d) 24. The h_y fields were chosen with respect to the threshold fields h_y^{thr} of the respective method. The red curve corresponds to the result of a 500×500 SBMFT cluster for comparison.

while in the full calculation the interplay of a huge number of multiple modes per momentum leads to enhanced interference.

In Figs. 7 and 8 the time evolution of the sublattice magnetization obtained from ED and SBMFT is depicted for the different clusters for $\chi = 0.5$ and $\chi = 0.8$, respectively. In all cases, the h_y values are chosen with respect to the threshold field of the corresponding approach, i.e., ED or SBMFT. The green curves refer to fields 20 % below and the blue curves to fields 20 % above the switching

threshold values of the respective method. In interpreting the shown data, one should keep in mind that there is some spurious dynamics even without switching field due to the turned off auxiliary field, see Fig. 4. Obviously, this spurious dynamics is negligible for $\chi = 0.5$ for the times displayed in Figs. 7 and 8. But for $\chi = 0.8$, this effect is not completely negligible, at least for the 4×4 cluster.

A comparison of the time evolution of magnetization resulting from the two approaches reveals similarities and differences. Figures 7 and 8 display the dynamics of the magnetization for the results of the ED (solid lines) and the SBMFT (dashed lines). The initial dynamics up to $t \approx 2/J$ is in good agreement and we will analyze it in more detail below. For longer times, however, deviations prevail. The ED results are considerably flatter, i.e., they do not show strong oscillations after the switching field has been turned on, while the SBMFT results oscillate significantly stronger on the displayed time scales. We attribute this difference to the difference in interference. The ED calculations allow for the superposition for tremendously more eigen modes since the full Hilbert space increases exponentially with system size. In contrast, the mean-field results only allow for interference of modes characterized by their wave number. Thus, this number of modes only increases proportional to the system size. Note that the increase of the system size in panels a) does not have a large impact up to moderate times $\approx 5/J$. But for longer times the increased destructive interference is discernible.

B. The magnetic field threshold for switching

Here we investigate the required minimum external field, to which we refer to as “threshold” field h_y^{thr} , to achieve the desired switching of the sublattice magnetization. For a proper comparison, the estimated auxiliary h_z fields from the exact diagonalization are also used for the Schwinger boson mean-field theory to determine the switching thresholds. In Fig. 9 the obtained switching thresholds for the rectangular clusters are shown. The data from the SBMFT are drawn as solid lines. A comparison to a very large system of 500×500 sites is depicted as a red solid line.

Within the range of $\chi \in [0.4, 0.8]$ where both methods are well applicable, they yield the same shape with a nearly constant deviation. At $\chi = 0.8$ the threshold field for the 4×4 lattice suddenly starts to increase, which was observed for both methods. We attribute this to strong finite-size effects so that this region is not physically relevant. If the system size is increased to 6×4 spins, the sudden increase of the threshold field is shifted to a higher value of $\chi \approx 0.88$. This tendency corroborates the view that these artifacts vanish for an infinitely large system. We expect that the shape of the threshold curve follows the shape of the red solid curve obtained from SBMFT for a 500×500 system. In the range

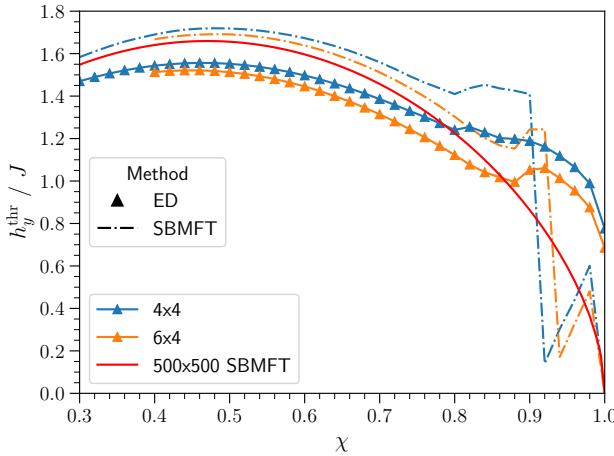


FIG. 9. Comparison of the threshold fields depending on the anisotropy factor χ for the 4×4 and the 6×4 spins clusters. The data for χ larger than 0.8 (0.88) is strongly affected by finite-size effects for the 4×4 (6×4) cluster.

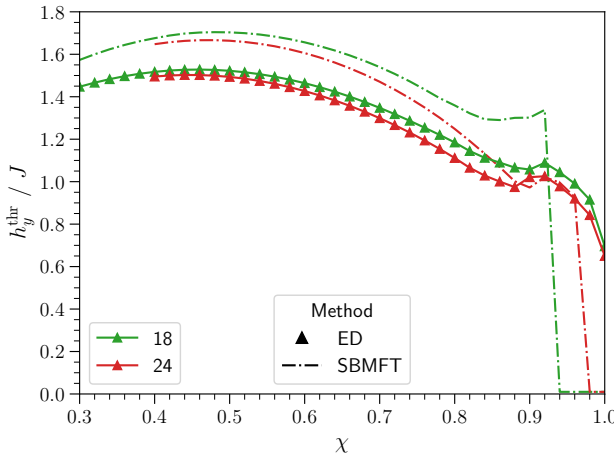


FIG. 10. Comparison of the threshold fields depending on the anisotropy factor χ for the 18 and the 24 rhombohedral spin clusters. The data for χ larger than 0.8 (0.88) is strongly affected by finite-size effects for the 18 (24) cluster.

$\chi \in [0.4, 0.8]$ the results of the exact diagonalization and the Schwinger boson mean-field theory are in good agreement. The deviation is in the range of about 12.5%. This finding strongly supports the applicability of SBMFT to obtain a good understanding of the temporal evolution on a semi-quantitative level.

Inspecting the rhombohedral clusters, see App. B for their shape, in Fig. 10 the same key points can be noticed. The shape of the threshold curve between $\chi \in [0.4, 0.88]$, as illustrated in Fig. 10, is reproduced by the SBMFT with an accuracy comparable to the one for the rectangular clusters. Also the strong finite-size effects set in at similar values of the anisotropy. These findings

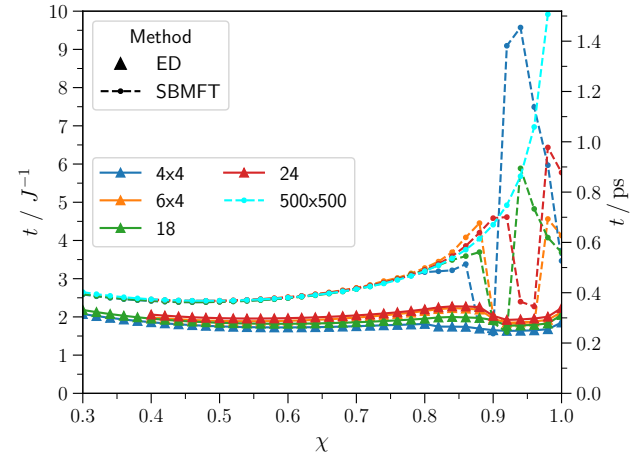


FIG. 11. Switching times depending on the anisotropic factor χ for the different clusters, where the switching h_y are chosen 20 % higher than the respective threshold fields h_y^{thr} of the method used. The y axis on the right indicates the switching times in picoseconds assuming a coupling strength of $J = 10$ meV.

corroborate the above conclusion that SBMFT is a well-applicable semi-quantitative approach for switching processes.

We add an explanation for the perhaps puzzling finite threshold field at $\chi = 1$ where one naively expects that no activation energy needs to be overcome. This is indeed true for infinite systems [12]. But for the finite clusters there is always a finite spin gap, see panel b) of Fig. 5, and hence always an activation energy to be overcome. Moreover, we point out that we use auxiliary fields to ensure a finite sublattice magnetization in the initial state. This puts the expectations for the isotropic antiferromagnetic clusters into perspective.

C. Switching times from ED and SBMFT

In Fig. 11 the switching times of the ED and SBMFT are shown. Besides the minimal required fields h_y^{thr} these times are relevant and characteristic quantities for the manipulation of the antiferromagnetic order parameters. We determine the switching times from the first minimum of $m_z(t)$ once $m_z(t)$ has undergone a sign change, see Figs. 7 and 8. In order not to be influenced by irrelevant fine-tuning we consider successful switching processes by choosing fields 20 % above the threshold fields as determined for the respective method, ED or SBMFT.

Passing from $\chi = 0.30$ to about $\chi = 0.60$ in the ED case, the switching times decrease until they reach a minimum which differs slightly from cluster to cluster. If χ is increased further to 0.80 the switching times start to rise again, until the detrimental finite-size effects start to show up as discussed in the Fig. 9. In the large N limit, i.e., in the thermodynamic limit, these effects are

expected to vanish. Thus, we expect that the dependence of the switching times on χ has a positive curvature with a minimum at around $\chi \approx 0.6$ for the infinite system.

For $\chi \rightarrow 1$, the SBMFT results for the large 500×500 cluster indicate a divergence of the switching times. This is indeed realistic because in the isotropic limit the switching fields become smaller and smaller eventually vanishing for $\chi = 1$. As a consequence the switching based on the Larmor precession about the switching field takes longer and longer so that the switching times diverge. This can be avoided by using staggered switching fields exploiting exchange-enhancement [14]. But this is beyond the scope of the present paper.

A comparison to the switching times of the SBMFT shows similar behavior. Passing from $\chi = 0.3$ up to roughly $\chi = 0.5$ the switching times decrease and start to increase as χ is becoming larger. At around $\chi = 0.8$ the switching times heavily oscillate as a consequence of the finite size clusters. Keep in mind that the switching fields depend on χ as well. This finite-size effect can also be observed for the other clusters at slightly larger χ values. The switching times are in reasonable agreement with the ED values with deviation of about 30% for the larger clusters. In particular the qualitative shape of their dependence is alike. Yet, the SBMFT yields higher switching times than the ED calculations. Inspecting Figs. 7 and 8 the deviation can be understood. While the first zero of $m_z(t)$ occurs quite early and matches very well between ED and SBMFT the subsequent minimum appears naturally later where the results of both approaches differ. Since the ED curves are flatter overall their minimum tends to occur earlier than the minimum in the SBMFT curve displaying larger oscillations.

Since antiferromagnetic storage devices are expected to allow for ultrafast switching times and hence for data manipulations in the range of THz, the estimated switching times are also converted to SI units. On the right y axis of Fig. 11 the switching times are given in picoseconds assuming a coupling strength of $J = 10$ meV. In this case, they are in the range of $0.25 - 0.5$ ps for $\chi < 0.8$. Even if one assumes a coupling strength of only $J = 1$ meV the switching times would still be in the range of $2.5 - 5$ ps. Therefore, the ultra fast switching capabilities of antiferromagnets are confirmed by both computational methods to be in the THz range.

IV. CONCLUSION

The presented theoretical results provide a comprehensive description of a switching process in quantum antiferromagnets by means of external magnetic fields. Using exact numerical calculations for small clusters, we have theoretically confirmed that the reorientation of the Néel vector is possible on an ultrafast time scale. Due to the finite size effects, the reliable computation of the temporal evolution of the field-driven quantum state is limited to short time scales.

Our comparison of the ED and SBMFT results shows that both approaches yield similar dynamic behavior in small systems on short time scales. A minimum field strength is necessary to achieve switching. The behavior of this threshold switching field strongly depends on the anisotropy of the system. The results for the threshold fields from ED and from SBMFT agree well with only about 12.5% of deviation in the range of $\chi = [0.4 - 0.8]$. Moreover, the switching times are in picosecond regime in both approaches, but the differences between the methods are large of about 30%. The switching time scale in the picosecond range underlines the ultrafast magnetization dynamics of this manipulation of the long-range antiferromagnetic order parameter.

The long time evolution, however, of the sublattice magnetization agrees only qualitatively between both approaches. Due to the very large size of the Hilbert space, the ED calculations display stronger dephasing than the results from SBMFT, i.e., the ED curves are flatter. The SBMFT results also show dephasing in contrast to macrospin calculations. But the number of modes which contribute to a generic signal such as the sublattice magnetization grow only linear in system size. On the one hand, this constitutes a certain caveat. On the other hand, it must be kept in mind that the ED approach is unable to reach the system sizes that would allow reliable predictions for the thermodynamic limit.

In addition, the spin isotropic limit $\chi \rightarrow 1$ cannot be analyzed by ED because the finite-size effects become obstructively dominating. Yet the satisfactory agreement between SBMFT and ED for small systems and short times allows us to trust the physically reasonable SBMFT results in the isotropic limit [12]. Furthermore, our previous studies demonstrated that the threshold fields can be significantly reduced based on exchange-enhancement [14] and/or the application of time-dependent control fields [13].

Although applying the theoretically found high switching fields is far from trivial and difficult to conduct experimentally in the laboratory, our results provide evidence that switching can be achieved on picosecond time scales.

To conclude, the analyses in present article shows that the time-dependent Schwinger boson mean-field theory is a justified approach to treat the switching process in quantum antiferromagnets. The obtained results pave the way for further investigations of switching processes and the description of non-classical behavior of the Néel vector in field-driven quantum antiferromagnets. This will help to leverage the potential of antiferromagnets for data storage and data processing.

ACKNOWLEDGMENTS

We are grateful to Joachim Stolze for the helpful discussion. This work has been financially supported by the Deutsche Forschungsgemeinschaft (German Research Foundation) in project UH 90/14-2.

Appendix A: Finite sublattice magnetization ground state

Initializing a suitable ground state for the switching process is crucial in order to start with a finite sublattice magnetization state. This is why we address this issue further. For small clusters, such as the ones we are dealing with in this work, the ground state would always have neither a finite total magnetization nor a finite sublattice magnetization [42] without an external magnetic field applied. This is why we have to apply a small auxiliary magnetic field h_z in the z direction in order to achieve a finite value of m_z . For a discrete set of h_z values, the sublattice magnetization

$$m_z(h_z) = \langle \Psi_0 | S_0^z | \Psi_0 \rangle \quad (\text{A1})$$

is calculated. The state $|\Psi_0\rangle$ denotes the ground state of the system at the corresponding staggered h_z field. The sublattice magnetization m_z is only calculated for the spin with index 0, because the lattice is translationally invariant after the sublattice rotation. The calculation of the expectation value for each spin in the cluster would become too time consuming for $N = 24$. For clarification we highlight, that after the rotation of one sublattice, all spins are aligned by the magnetic field in the same direction. For the original unrotated system this corresponds to a staggered, antiferromagnetic alignment of the spins. For each χ , a few $m_z(h_z)$ values are calculated as exemplified in Fig. 3. Each blue dot corresponds to one ground state calculation performed in the $H_{(k_x, k_y)}$ subspace with ($k_x = 0, k_y = 0$) which is done using QuSpin.

In order to benefit from the translational invariance, we define equivalence classes. For a given unitary symmetry transformation Q with periodicity M , such that

$$Q^M = \mathbb{1} \quad , \quad (\text{A2})$$

the Hilbert space can be decomposed into equivalence classes, called cycles C_i . Each cycle

$$C_i = \{|\phi_i\rangle, Q|\phi_i\rangle, Q^2|\phi_i\rangle, \dots, Q^{L_i-1}|\phi_i\rangle\} \quad (\text{A3})$$

has length L_i and one representative state $|\phi_i\rangle$ from which all other states in this cycle can be reconstructed by means of Q . For each quantum number $m \in [0, 1, \dots, M-1]$ and representative $|\phi_i\rangle$, a new state

$$|m, \phi_i\rangle = \frac{1}{L_i} \sum_{n=0}^{L_i-1} e^{-i(\frac{2\pi m}{M})n} \hat{Q}^n |\phi_i\rangle \quad (\text{A4})$$

is defined. The corresponding eigenvalue equation reads

$$Q|m, \phi_i\rangle = e^{i\frac{2\pi m}{M}} |m, \phi_i\rangle \quad . \quad (\text{A5})$$

Then, the subspace can be constructed by computing $\langle m, \phi_i | \hat{H} | m, \phi_j \rangle$ for each quantum number m , using all different cycles C_i . Once the subspace is formed, the ground state is searched by using the so called "eigsh"

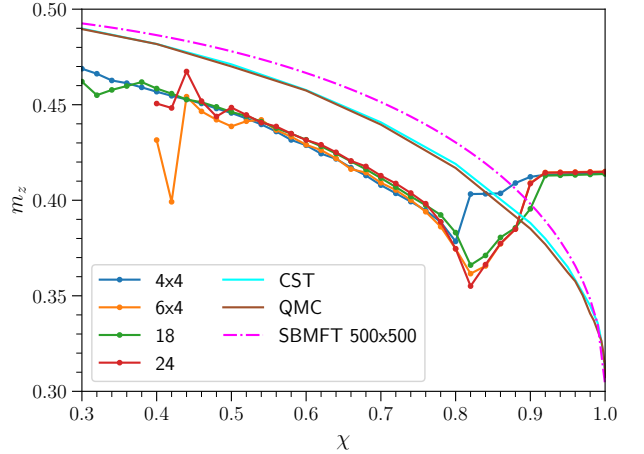


FIG. 12. Comparison of the ground state sublattice magnetization between our finite clusters and the continuous similarity transformation [43] method and the quantum Monte Carlo [52–54] approach in the thermodynamic limit without auxiliary h_z field.

sparse eigensolver from the SciPy linear algebra library. Once the sublattice magnetization values are calculated for different h_z fields, we use equation (14) to fit the magnetization. Then the normalized derivative according to (15) is calculated and the initial h_z field is determined.

To determine a suitable value for the auxiliary field, we require that the normalized derivative takes a value of 0.03, yielding an auxiliary h_z field value that is close to the point where the sublattice magnetization assumes its thermodynamics value. Still, this condition is chosen a bit arbitrarily, but set in a way such that the initial sublattice magnetization agrees reasonably with results from other methods shown in Fig. 12. This figure displays a comparison between our estimated ground state sublattice magnetization to the results of a continuous similarity transformation (CST) [43] and of a quantum Monte Carlo (QMC) [52–54] approach which provide results extrapolated to the thermodynamic limit. Our sublattice magnetization values underestimate the values of CST and QMC in the relevant low χ region. Note, however, that the SBMFT result for a large system slightly overestimates m_z for all χ values. Summarizing, the curvature of the graph is reproduced well up to a value of approximately $\chi = 0.8$ where severe mismatch sets in due to dominant finite-size effects.

The resulting auxiliary magnetic fields are shown in Fig. 13. For small values of χ , only a very tiny field is required in order to induce a finite sublattice magnetization ground state. This is because the quantum tunneling from one ordered state to the other is strongly suppressed so that both are almost perfectly degenerate. If the system becomes more isotropic, larger and larger magnetic fields are necessary to obtain the appropriate sublattice magnetization value.

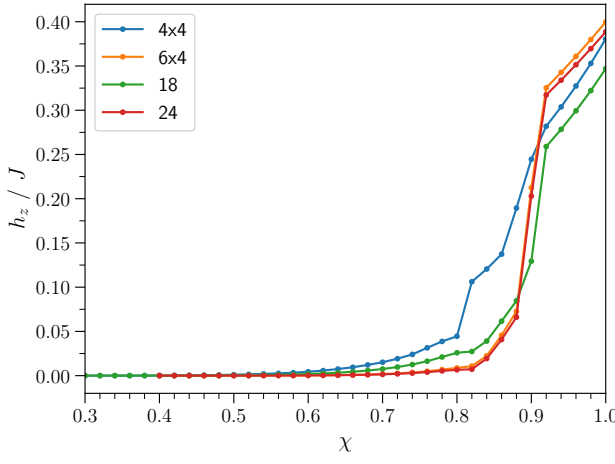


FIG. 13. Estimated auxiliary h_z fields as functions of the anisotropic factor χ for various clusters.

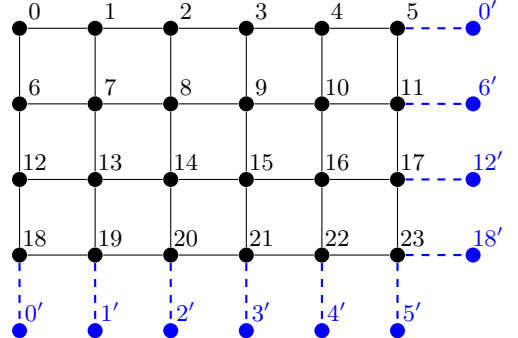


FIG. 15. 6×4 spin lattice

$$k_x = -\pi + n \frac{\pi}{2}, \quad n = 0, 1, 2, 3, 4, 5$$

$$k_y = -\pi + m \frac{\pi}{2}, \quad m = 0, 1, 2, 3$$

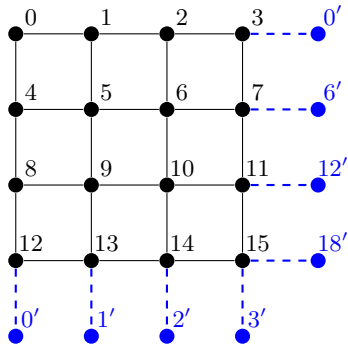


FIG. 14. 4×4 spin lattice

$$k_x = -\pi + n \frac{\pi}{2}, \quad n = 0, 1, 2, 3$$

$$k_y = -\pi + m \frac{\pi}{2}, \quad m = 0, 1, 2, 3$$

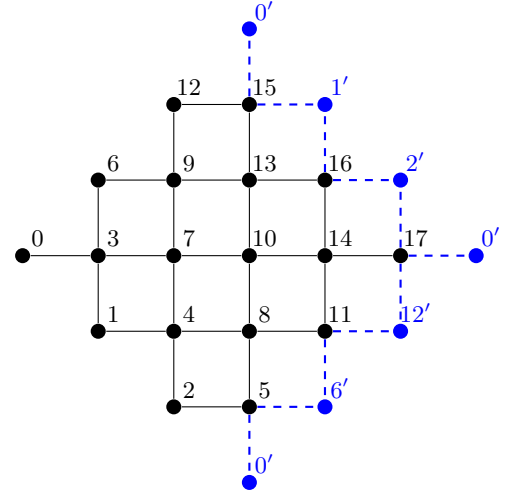


FIG. 16. 18 spin lattice

$$k_x = \frac{2\pi n}{6}, \quad n = 0, 1, 2, 3, 4, 5$$

$$k_y = \frac{\pi}{3} (2m - n), \quad m = 0, 1, 2$$

Appendix B: Lattice structures

Here, we provide the used lattice structures for our calculations, as well as the corresponding \mathbf{k} points in the reciprocal space. In every case periodic boundary conditions were used indicated by the blue dots with primed numbers.

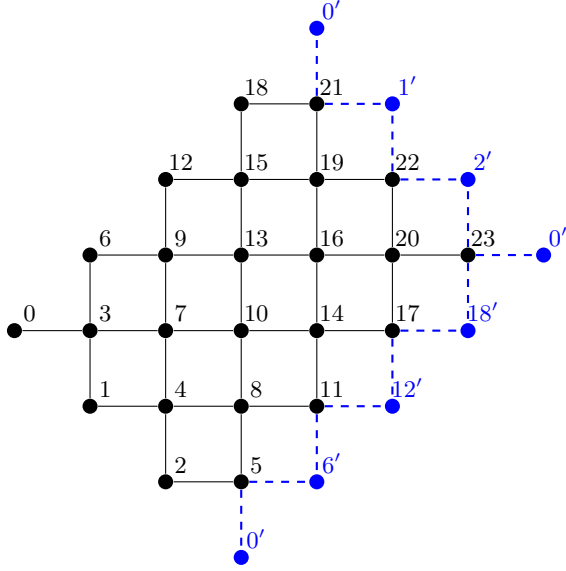


FIG. 17. 24 spin lattice

$$k_x = \frac{\pi}{2} \left(\frac{n}{3} + \frac{m}{2} \right), \quad n = 0, 1, 2, 3, 4, 5$$

$$k_y = \frac{\pi}{2} \left(\frac{m}{2} - \frac{n}{3} \right), \quad m = 0, 1, 2, 3$$

-
- [1] T. Jungwirth, X. Marti, P. Wadley, and J. Wunderlich, Antiferromagnetic spintronics, *Nature Nanotechnology* **11**, 231 (2016).
- [2] V. Baltz, A. Manchon, M. Tsoi, T. Moriyama, T. Ono, and Y. Tserkovnyak, Antiferromagnetic spintronics, *Review Modern Physics* **90**, 015005 (2018).
- [3] H. Qiu, L. Zhou, C. Zhang, Y. Wu, J. and Tian, S. Cheng, S. Mi, H. Zhao, Q. Zhang, D. Wu, B. Jin, J. Chen, and P. Wu, Ultrafast spin current generated from an antiferromagnet, *Nature Physics* **17**, 388 (2021).
- [4] E. Rongione, O. Gueckstock, M. Mattern, O. Gomonay, H. Meer, C. Schmitt, R. Ramos, T. Kikkawa, M. Mičica, E. Saitoh, J. Sinova, H. Jaffrè, J. Mangeney, S. T. B. Goennenwein, S. Geprägs, T. Kampfrath, M. Kläui, M. Bargheer, T. S. Seifert, S. Dhillon, and R. Lebrun, Emission of coherent THz magnons in an antiferromagnetic insulator triggered by ultrafast spin–phonon interactions, *Nature Communications* **14**, 1818 (2023).
- [5] A. H. MacDonald and M. Tsoi, Antiferromagnetic metal spintronics, *Philosophical Transactions of the Royal Society A: Mathematical, Physical and Engineering Sciences* **369**, 3098 (2011).
- [6] O. Gomonay, T. Jungwirth, and J. Sinova, Concepts of antiferromagnetic spintronics, *Physica Status Solidi (RRL)* **11**, 1700022 (2017).
- [7] M. B. Jungfleisch, W. Zhang, and A. Hoffmann, Perspectives of antiferromagnetic spintronics, *Physics Letters A* **382**, 865 (2018).
- [8] T. Jungwirth, J. Sinova, A. Manchon, X. Marti, J. Wunderlich, and C. Felser, The multiple directions of antiferromagnetic spintronics, *Nature Physics* **14**, 200 (2018).
- [9] A. Kimel, T. Rasing, and B. Ivanov, Optical read-out and control of antiferromagnetic Néel vector in altermagnets and beyond, *Journal of Magnetism and Magnetic Materials* **598**, 172039 (2024).
- [10] E. V. Gomonay and V. M. Loktev, Spintronics of antiferromagnetic systems (review article), *Low Temperature Physics* **40**, 17 (2014).
- [11] O. Gomonay, T. Jungwirth, and J. Sinova, High antiferromagnetic domain wall velocity induced by Néel spin-orbit torques, *Phys. Rev. Lett.* **117**, 017202 (2016).
- [12] K. Bolsmann, A. Khudoyberdiev, and G. S. Uhrig, Switching the magnetization in quantum antiferromagnets, *PRX Quantum* **4**, 030332 (2023).
- [13] A. Khudoyberdiev and G. S. Uhrig, Switching of magnetization in quantum antiferromagnets with time-dependent control fields, *Phys. Rev. B* **109**, 174419 (2024).
- [14] A. Khudoyberdiev and G. S. Uhrig, Exchange-enhanced switching by alternating fields in quantum antiferromagnets, *Phys. Rev. B* **111**, 064408 (2025).
- [15] M. Yarmohammadi, P. M. Oppeneer, and J. K. Freericks, Cavity-assisted magnetization switching in a quantum spin-phonon chain, *Phys. Rev. B* **112**, 094445 (2025).
- [16] J. Železný, H. Gao, K. Výborný, J. Zemen, J. Mašek, A. Manchon, J. Wunderlich, J. Sinova, and T. Jungwirth, Relativistic Néel-order fields induced by electrical current in antiferromagnets, *Physical Review Letters* **113**,

- 157201 (2014).
- [17] J. Železný, H. Gao, A. Manchon, F. Freimuth, Y. Mokrousov, J. Zemen, J. Mašek, J. Sinova, and T. Jungwirth, Spin-orbit torques in locally and globally noncentrosymmetric crystals: Antiferromagnets and ferromagnets, *Physical Review B* **95**, 014403 (2017).
- [18] S. Y. Bodnar, L. Šmejkal, I. Turek, T. Jungwirth, O. Gomonay, J. Sinova, a. A. Sapozhnik, H.-J. Elmers, M. Kläui, and M. Jourdan, Writing and reading antiferromagnetic Mn₂Au by Néel spin-orbit torques and large anisotropic magnetoresistance, *Nature Communications* **9**, 348 (2018).
- [19] Y. Behovits, A. L. Chekhov, S. Y. Bodnar, O. Gueckstock, S. Reimers, Y. Lytvynenko, Y. Skourski, M. Wolf, T. S. Seifert, O. Gomonay, M. Kläui, M. Jourdan, and T. Kampfrath, Terahertz Néel spin-orbit torques drive nonlinear magnon dynamics in antiferromagnetic Mn₂Au, *Nature Communications* **14**, 6038 (2023).
- [20] P. Wadley, B. Howells, J. Železný, C. Andrews, V. Hills, R. P. Campion, V. Novák, K. Olejník, F. Maccherozzi, S. S. Dhesi, S. Y. Martin, T. Wagner, J. Wunderlich, F. Freimuth, Y. Mokrousov, J. Kuneš, J. S. Chauhan, M. J. Grzybowski, A. W. Rushforth, K. W. Edmonds, B. L. Gallagher, and T. Jungwirth, Electrical switching of an antiferromagnet, *Science* **351**, 587 (2016).
- [21] L. Han, X. Fu, R. Peng, X. Cheng, J. Dai, L. Liu, Y. Li, Y. Zhang, W. Zhu, H. Bai, Y. Zhou, S. Liang, C. Chen, Q. Wang, X. Chen, L. Yang, Y. Zhang, C. Song, J. Liu, and F. Pan, Electrical 180° switching of Néel vector in spin-splitting antiferromagnet, *Science Advances* **10**, eadn0479 (2024).
- [22] H. Guo, Z. Lin, J. Lu, C. Yun, G. Han, S. Sun, Y. Wu, W. Yang, D. Xiao, Z. Zhu, L. Peng, Y. Ye, Y. Hou, J. Yang, and Z. Luo, Layer-dependent spin-orbit torque switching of Néel vector in a van der Waals antiferromagnet, *Nature Communications* **16**, 8911 (2025).
- [23] S. P. Bommanaboyena, D. Backes, L. S. I. Veiga, S. S. Dhesi, Y. R. Niu, B. Sarpi, T. Denneulin, A. Kovács, T. Mashoff, O. Gomonay, J. Sinova, K. Everschor-Sitte, D. Schönke, R. M. Reeve, M. Kläui, H.-J. Elmers, and M. Jourdan, Readout of an antiferromagnetic spintronics system by strong exchange coupling of Mn₂Au and Permalloy, *Nature Communications* **12**, 6539 (2021).
- [24] V. Grigorev, M. Filianina, S. Y. Bodnar, S. Sobolev, N. Bhattacharjee, S. Bommanaboyena, Y. Lytvynenko, Y. Skourski, D. Fuchs, M. Kläui, M. Jourdan, and J. Demsar, Optical readout of the Néel vector in the metallic antiferromagnet Mn₂Au, *Physical Review Applied* **16**, 014037 (2021).
- [25] S. Ghara, M. Winkler, S. W. Schmid, L. Prodan, K. Geirhos, V. Tsurkan, W. Ge, W. Wu, A. Halbritter, S. Krohns, and I. Kézsmárki, Nonvolatile electric control of antiferromagnetic states on nanosecond timescales, *Phys. Rev. Lett.* **135**, 126704 (2025).
- [26] V. Polewczyk, A. Y. Petrov, B. Sarpi, D. Backes, H. El-naggar, P. Wadhwa, A. Filippetti, G. Rossi, P. Torelli, G. Vinai, F. Maccherozzi, and B. A. Davidson, Control of the antiferromagnetic domain configuration and néel axis orientation with epitaxial strain, *Communications Materials* **6**, 153 (2025).
- [27] S. Toyoda, V. Kocsis, Y. Tokunaga, I. Kézsmárki, Y. Taguchi, T.-h. Arima, Y. Tokura, and N. Ogawa, All-optical control of antiferromagnetic domains via an inverse optical magnetoelectric effect, arXiv (2025), submitted on 8 Jun 2025, arXiv:2506.07051 [cond-mat.mtrl-sci].
- [28] M. Jourdan, G. O. Bläser, J. and Gámez, S. Reimers, L. Odenbreit, M. Fischer, Y. R. Niu, E. Golias, F. Maccherozzi, A. Kleibert, H. Stoll, and M. Kläui, Identifying switching of antiferromagnets by spin-orbit torques, *Phys. Rev. B* **112**, 104408 (2025).
- [29] X. Chen, X. Zhou, R. Cheng, C. Song, J. Zhang, Y. Wu, Y. Ba, H. Li, Y. Sun, Y. You, Y. Zhao, and F. Pan, Electric field control of Néel spin-orbit torque in an antiferromagnet, *Nature Materials* **18**, 931 (2019).
- [30] H. V. Gomonay and V. M. Loktev, Spin transfer and current-induced switching in antiferromagnets, *Physical Review B* **81**, 144427 (2010).
- [31] G. S. Uhrig, Landau–Lifshitz damping from Lindbladian dissipation in quantum magnets, *New Journal of Physics* **27**, 103502 (2025).
- [32] J. L. Ross, P.-I. Gavrilaea, F. Freimuth, T. Adamantopoulos, Y. Mokrousov, R. F. L. Evans, R. Chantrell, R. M. Otxoa, and O. Chubykalo-Fesenko, Ultrafast antiferromagnetic switching of Mn₂Au with laser-induced optical torques, *npj Computational Materials* **10**, 234 (2024).
- [33] T. Holstein and H. Primakoff, Field dependence of the intrinsic domain magnetization of a ferromagnet, *Physical Review* **58**, 1098 (1940).
- [34] F. J. Dyson, General theory of spin-wave interactions, *Physical Review* **102**, 1217 (1956).
- [35] S. V. Maleev, Scattering of slow neutrons in ferromagnets, *Soviet Physics JETP* **6**, 766 (1958).
- [36] A. Rückriegel, A. Kreisel, and P. Kopietz, Time-dependent spin-wave theory, *Physical Review B* **85**, 054422 (2012).
- [37] J. Schwinger, US Atomic Energy Commission 10.2172/4389568.
- [38] A. Khudoyberdiev and G. S. Uhrig, The effect of dephasing and spin-lattice relaxation during the switching processes in quantum antiferromagnets, *SciPost Phys.* **19**, 117 (2025).
- [39] H.-P. Breuer and F. Petruccione, *The Theory of Open Quantum Systems* (Clarendon Press, Oxford, 2006).
- [40] C. Beckmann and J. Schnack, Investigation of thermalization in giant-spin models by different Lindblad schemes, *J. Mag. Mag. Mat.* **437**, 7 (2017).
- [41] A. Lüscher and A. M. Läuchli, Exact diagonalization study of the antiferromagnetic spin- $\frac{1}{2}$ Heisenberg model on the square lattice in a magnetic field, *Phys. Rev. B* **79**, 195102 (2009).
- [42] E. Lieb and D. Mattis, Theory of ferromagnetism and the ordering of electronic energy levels, *Phys. Rev.* **125**, 164 (1962).
- [43] N. Caci, D.-B. Hering, M. R. Walther, K. P. Schmidt, S. Wessel, and G. S. Uhrig, Quantitative description of long-range order in the spin- $-\frac{1}{2}$ XXZ antiferromagnet on the square lattice, *Phys. Rev. B* **110**, 054411 (2024).
- [44] A. Auerbach, *Interacting Electrons and Quantum Magnetism*, Graduate Texts in Contemporary Physics (Springer, New York, 1994).
- [45] M. Raykin and A. Auerbach, 1/N expansion and spin correlations in constrained wave functions, *Physical Review B* **47**, 5118 (1993).
- [46] A. S. T. Pires, *Theoretical Tools for Spin Models in Magnetic Systems*, 2053-2563 (IOP Publishing, 2021).

- [47] B. Fauseweh and J.-X. Zhu, Ultrafast optical induction of magnetic order at a quantum critical point, *J. Phys.: Condens. Matter* **37**, 075603 (2024).
- [48] P. Weinberg and M. Bukov, QuSpin: a Python package for dynamics and exact diagonalisation of quantum many body systems part I: spin chains, *SciPost Phys.* **2**, 003 (2017).
- [49] P. Weinberg and M. Bukov, QuSpin: a Python package for dynamics and exact diagonalisation of quantum many body systems. Part II: bosons, fermions and higher spins, *SciPost Phys.* **7**, 020 (2019).
- [50] R. Cheng, M. W. Daniels, J.-G. Zhu, and D. Xiao, Ultrafast switching of antiferromagnets via spin-transfer torque, *Phys. Rev. B* **91**, 064423 (2015).
- [51] M. Weißenhofer, F. Foggetti, U. Nowak, and P. M. Oppeneer, Néel vector switching and terahertz spin-wave excitation in Mn_2Au due to femtosecond spin-transfer torques, *Phys. Rev. B* **107**, 174424 (2023).
- [52] A. W. Sandvik and J. Kurkijärvi, Quantum Monte Carlo simulation method for spin systems, *Phys. Rev. B* **43**, 5950 (1991).
- [53] A. W. Sandvik, Stochastic series expansion method with operator-loop update, *Phys. Rev. B* **59**, R14157 (1999).
- [54] O. F. Syljuåsen and A. W. Sandvik, Quantum Monte Carlo with directed loops, *Phys. Rev. E* **66**, 046701 (2002).